metals

MDPI

Article

Influence of Heat Control on Properties and Residual Stresses of Additive-Welded High-Strength Steel Components

Ronny Scharf-Wildenhain [1,*], André Haelsig [1], Jonas Hensel [1], Karsten Wandtke [2], Dirk Schroepfer [2], Arne Kromm [2] and Thomas Kannengiesser [2]

[1] Welding Technology, Chemnitz University of Technology, D-09107 Chemnitz, Germany; andre.haelsig@mb.tu-chemnitz.de (A.H.); jonas.hensel@mb.tu-chemnitz.de (J.H.)
[2] Bundesanstalt fuer Materialforschung und -pruefung (BAM), D-12205 Berlin, Germany; karsten.wandtke@bam.de (K.W.); dirk.schroepfer@bam.de (D.S.); arne.kromm@bam.de (A.K.); thomas.kannengiesser@bam.de (T.K.)
* Correspondence: ronny.scharf-wildenhain@mb.tu-chemnitz.de

Abstract: Advanced high-performance filler metals for wire arc additive manufacturing (WAAM) exist on the market already. Nevertheless, these high-strength steels are not yet widely used in industrial applications due to limited knowledge of cold-cracking susceptibility, welding residual stresses, and therefore sufficient safety in terms of manufacturing and operation. High residual stresses promote cold-cracking risk, especially in the welding of high-strength steels, as the result of a complex interaction between the applied material, process conditions, and component design. The focus of the present investigation was the determination of the influence of the process parameters on the $\Delta t_{8/5}$ cooling time, mechanical properties, and residual stresses to correlate, for the first time, heat control, cooling conditions, and residual stress for WAAM of high-strength filler materials. This contributed to the knowledge regarding the safe avoidance of cold cracking. In addition to a thermophysical simulation using a dilatometer of different high-strength steels with subsequent tensile testing, reference WAAM specimens (open hollow cuboids) were welded while utilizing a high-strength filler metal (ultimate tensile strength > 790 MPa). The heat control was varied by means of the heat input and interlayer temperature such that the $\Delta t_{8/5}$ cooling times corresponded to the recommended processing range (approx. 5 s to 20 s). For the heat input, significant effects were exhibited, in particular on the local residual stresses in the component. Welding with an excessive heat input or deposition rate may lead to low cooling rates, and hence to unfavorable microstructure and component properties, but at the same time, is intended to result in lower tensile residual stress levels. Such complex interactions must ultimately be clarified to provide users with easily applicable processing recommendations and standard specifications for an economical WAAM of high-strength steels. These investigations demonstrated a major influence of the heat input on both the cooling conditions and the residual stresses of components manufactured with WAAM using high-strength filler materials. A higher heat input led to longer cooling times ($\Delta t_{8/5}$) and approx. 200 MPa lower residual stresses in the surface of the top layer.

Keywords: WAAM; additive manufacturing; heat control; high-strength filler metals; residual stress

Citation: Scharf-Wildenhain, R.; Haelsig, A.; Hensel, J.; Wandtke, K.; Schroepfer, D.; Kromm, A.; Kannengiesser, T. Influence of Heat Control on Properties and Residual Stresses of Additive-Welded High-Strength Steel Components. *Metals* **2022**, *12*, 951. https://doi.org/10.3390/met12060951

Academic Editor: Alberto Campagnolo

Received: 28 April 2022
Accepted: 27 May 2022
Published: 31 May 2022

1. Introduction

Additive manufacturing (AM) processes enable engineers and designers to break new ground in the direct implementation of lightweight construction principles. In particular, the use of modern high-strength structural steels allows the design of lightweight components with low wall thicknesses and high-performance component properties. A weight reduction of 78% can be achieved by simply exchanging a conventional S235J2 with an S960QL [1,2]. The efficient use of materials and energy can reduce industrial emissions of greenhouse gases in order to achieve the national and international climate protection

targets [3]. With AM of high-strength materials in particular a full exploitation of the lightweight construction potential of technical applications in the areas of system, function, structure, and material is achievable [4]. A further increase in efficiency can be achieved through near-net-shape production [5].

The basic applicability of WAAM in the production of complex and large components with industrial robots has been proven in various works [4–6]. For a large-scale economic industrial application, there is a lack of quantitative information on the manufacturing-related stresses and structural reliability during component production and operation. This involves extensive investigations of the complex interactions between the welding process, especially heat control by means of the welding thermal cycle, the metallurgical processes, and design aspects, with the aim of reliably avoiding high tensile residual stresses. Similar to conventional joint welding, high tensile residual stresses are detrimental regarding cold cracking and also premature component failure, especially for high-strength materials. For welded joints, stress optimization by means of adapted heat-control concepts have already been the subject of research. Schroepfer et al. demonstrated the major influence of heat control on the formation of welding residual stresses [7]. It was shown that the interpass temperature in particular affected the global reactions stresses that were superimposed with local welding stresses, and the heat input predominantly influenced the cooling time and weld microstructure. However, systematic studies on their transferability to AM for high-strength steels are still lacking. Hoennige et al. investigated welding stresses in WAAM components of Ti6Al-4V and demonstrated that it was possible to reduce longitudinal residual stresses and distortion using side rolling [8]. Although manufacturing-related stresses in structural steel WAAM components have already been the subject of research by Denkena et al. [9], these have not yet been considered in the context of the special microstructures and low ductility reserves of high-strength steels and the effect of the welding parameters on the residual stresses. Depending on the component dimensions, ready-to-use WAAM welding systems are now commercially available in various sizes, and can be used to generate components automatically [10]. In addition, studies demonstrated the suitability and efficiency of the controlled MSG short arc (e.g., cold metal transfer (CMT) or ColdArc) for large components [11]. Different studies dealt with the strong dependence of the temperature distribution and the resulting component geometry on the welding parameters [12–14]. These investigations showed the great importance of heat control in setting the desired microstructural properties of high-strength steels using WAAM. Graf et al. investigated the influence of the wire feed rate and build-up strategy (continuous or discontinuous) on temperature development during WAAM [12]. These investigations confirmed the great influence of the build-up strategy and component geometry on temperature accumulation in WAAM components. The relatively narrow processing range in high-strength steel welding; e.g., cooling time $\Delta t_{8/5}$ for S690: 5 to 20 s, involves limited heat control parameters in order to achieve low manufacturing-related stresses, and at the same time, adequate microstructures with low cold cracking susceptibility and sufficient mechanical properties. This can be achieved by adjusting the heat input: preheating and interlayer temperature in such a way that as little heat as possible is introduced in the component during production [13]. In addition, Mueller et al. showed the influence of welding parameters on the mechanical–technological properties of WAAM-manufactured components [14]. The results indicated a lower yield strength and an increased tensile strength when welding with a higher heat input.

It should be emphasized that the use of high-strength structural steels has great potential in WAAM. The process-related residual stresses and material-related low ductility reserves, combined with the high welding requirements, result in a high risk of cold cracking. Therefore, residual stress analyses of the AM components are necessary to evaluate the influence of the material and design aspects and of the process conditions. Various methods can be used for this, such as X-ray diffraction and the incremental hole-drilling method for residual stresses near the surface [15,16]. Due to the limitations of drilling methods, which only provide reliable measurements up to approx. 60% of the

material yield strength, nondestructive analysis by means of XRD should be used whenever it is to be assumed that measured values in the yield strength range are to be detected. Since the penetration depth of the X-rays is only a few micrometers, only the residual stresses near the surface can be determined. In research, other methods are commonly used for comparison purposes, especially in the determination of welding residual stresses in the bulk [15]. These include, for example, the contour method, neutron and synchrotron diffraction, the dissection technique, or the so-called deep-hole drilling [17]. Several investigations of AM components showed that high residual stresses and residual stress gradients could be expected, especially on the component surfaces [18,19], which also were in the range of the material yield strength. Due to this, as well as the fact that high tensile residual stresses; e.g., at notches, have a detrimental effect on the cold-cracking risk and performance of the component, investigations of the residual stresses should initially be analyzed predominantly by means of XRD. However, to date, no studies in this regard have been carried out to prevent cold cracking in WAAM processing of high-strength structural steels in the context of the evolution (magnitude and distribution) of welding stresses in realistic component dimensions. However, such knowledge is crucial for economic application, since the applicability of postweld heat treatment for residual stress reduction in these high-strength steels is only limited by economic and metallurgical aspects due to the special microstructures.

In this context, this study dealt with the fundamental relationships between the welding parameters and additive build-up strategy on the resulting cooling rates, mechanical properties, and residual stresses. This investigation was part of a joint project of the Chemnitz University of Technology and BAM (FOSTA P1380/IGF 21,162 BG).

2. Materials and Methods

2.1. WAAM Welding System

For the welding tests, a robot-assisted WAAM cell consisting of a KUKA industrial robot and Fronius welding power source was implemented at the Chemnitz University of Technology, cf. Figure 1. The robot program installed on the controller contained all movement commands for the robot arm (manipulator) and for the welding power source. The controller evaluated the program and sent the corresponding motion and welding commands to both the manipulator and the welding power source via a corresponding interface. In the present study, a controlled short arc was used with the parameters of welding speed (travel speed of the robot), wire feed rate, arc correction, and dynamic factors.

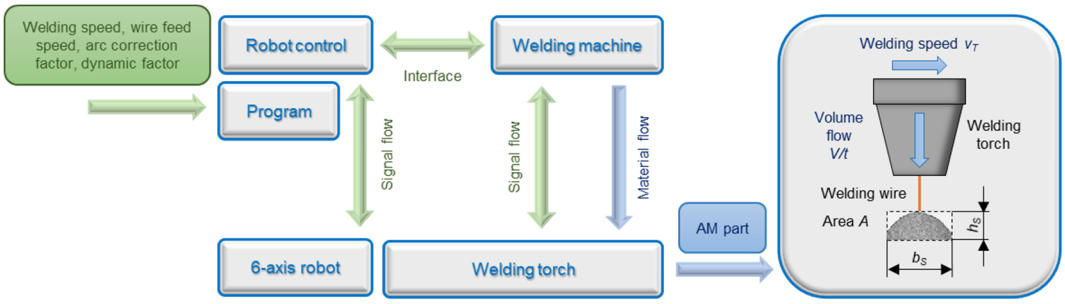

Figure 1. Simplified block diagram of the implemented WAAM cell at the Chemnitz University of Technology; layer width b_S and height h_S were set indirectly via the welding parameters of welding speed v_T and volume flow per time V/t.

The path coordinates for additive manufacturing were basically derived from a CAD model using slicers and translated into executable welding programs using a specially developed compiler. The workflow for the manufacturer-independent generation of executable robot programs, as well as the required software, were developed and successfully used in independent projects at the Chemnitz University of Technology.

2.2. Materials

In this project, a high-strength WAAM-optimized filler metal with a strength class of 790 MPa and a diameter of 1.2 mm was used. In contrast to conventional high-strength filler materials of the same strength (e.g., G 79 5 M21 Mn4Ni1.5CrMo), this material has stabilizing alloying elements that ensure WAAM-optimized melting conditions. With regard to welding heat control, this ensured an extended processing window while also ensuring the required mechanical properties. The WAAM specimen's reference geometries were built on a 30 mm thick steel substrate plate of S690QL with a yield strength of 690 MPa. In accordance with the recommendations of the steel manufacturers, this material combination allows adequate bonding of the AM component to the substrate plate within the selected experimental design. In this way, the necessary ductility in the transition area and, at the same time, an adequately high strength of the substrate in connection with a sufficiently high stiffness or restraint condition close to real applications were realized when WAAM-welding the component specimens.

For the thermophysical welding and forming simulation, in addition to the above-mentioned materials, samples of S960QL were also investigated in order to be able to compare the behavior of the novel WAAM filler metal with conventional high-strength structural steels. Table 1 shows the chemical compositions and mechanical properties of all test materials.

Table 1. Mechanical properties and chemical composition (in wt%, Fe-balanced) of the filler and the base metals investigated in the recommended $\Delta t_{8/5}$ range of 5 s to 20 s based on material test certificates.

Material	Chemical Composition						Mechanical Properties		
	C	Mn	Si	Mo	Cr	Ni	$R_{p0.2}$	R_m	A_5
WAAM wire	0.09	1.70	0.40	0.60	0.35	2.00	820 MPa	920 MPa	20%
S690QL (1.8931)	0.14	1.15	0.30	0.17	0.30	0.10	771 MPa	824 MPa	17%
S960QL (1.8933)	0.17	0.88	0.27	0.52	0.49	0.51	1039 MPa	1059 MPa	15%

2.3. Thermophysical Welding and Forming Simulation with Dilatometer

In this investigation, the fine-grained structural steels S690QL (1.8931) and S960QL (1.8933) and the novel WAAM wire were comparatively analyzed. To obtain detailed results on the ultimate tensile strength as a function of the $\Delta t_{8/5}$ cooling time, tests were carried out to thermophysically simulate a welding process. In the test series, sheet specimens were subjected to one time–temperature cycle (load-free) based on WAAM welding (Figure 2, left). After cooling to room temperature (RT) defined by the $\Delta t_{8/5}$ cooling time, the sheet specimens were subjected to a tensile test (test speed 10 mm/min) in the same setup, cf. Figure 2. These tests were used to determine the influence of varying cooling rates on the tensile strength of the materials. The peak temperature of the time–temperature cycles was 1200 °C, and the $\Delta t_{8/5}$ cooling time was varied between 1.5 s and 45 s.

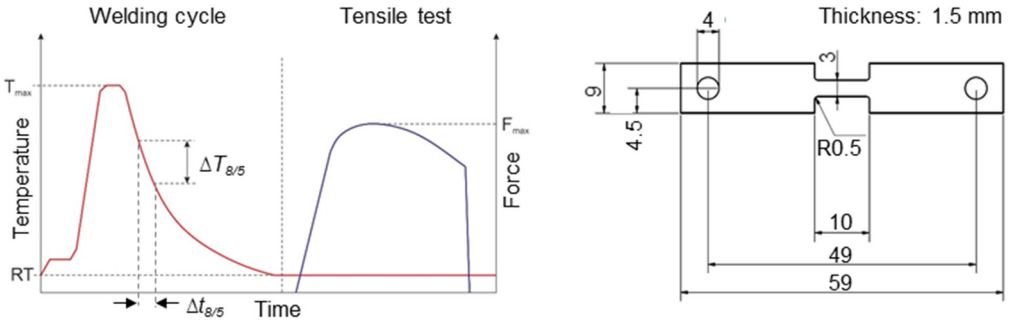

Figure 2. Schematic representation of the test sequence of the thermomechanical simulation (**left**) and specimen geometry of the sheet specimens used (**right**).

2.4. Welding Experiments

The layer width b_S and height h_S were set indirectly via the welding parameters (welding speed v_T and volume flow per time V/t), cf. Figure 1. Consequently, these parameters were the main influencing variables on the generated material cross-section [4]. At the same time, the welding parameters influenced the heat input into the WAAM component, and thus also the behavior of the metallic melt during processing. The described welding tests were performed to examine the interactions between welding parameters, cooling conditions, and residual stresses on identical specimen dimensions.

For this purpose, a total of nine geometrically identical open hollow cuboids were fabricated and investigated under systematic (full factorial) variations in the interlayer temperature (100 °C, 200 °C, and 300 °C) and heat input (200 kJ/m, 425 kJ/m, and 650 kJ/m), cf. Figure 3. The cooling times were determined during welding by means of temperature measurements with thermocouples (type-K).

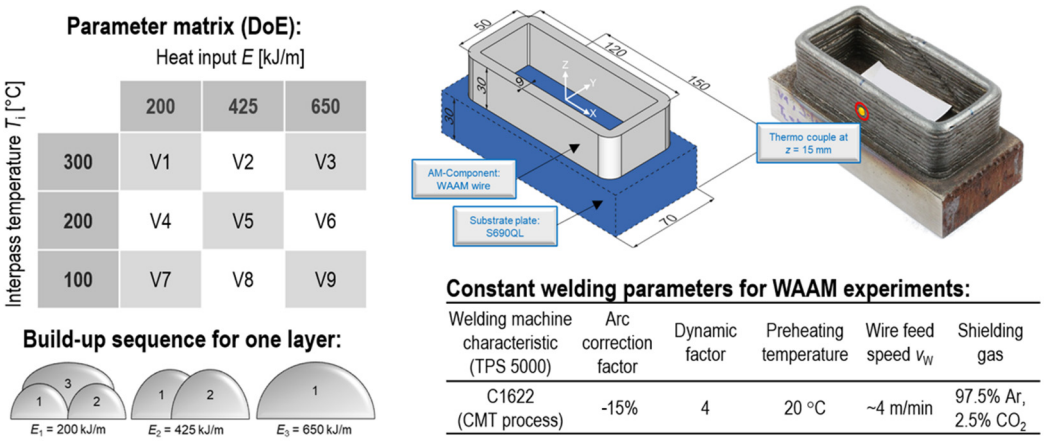

(**a**) (**b**)

Figure 3. (**a**) Parameter matrix and build-up sequence for 9 mm wide layer for WAAM experiments; (**b**) specification of the reference geometry (open hollow cuboid): CAD model (**left**), weld result (**right**), welding parameters (**bottom**).

2.5. Residual Stress Analysis

The analysis of local residual stresses was performed via X-ray diffraction (XRD) transverse and longitudinal to the welding direction using the $\sin^2\psi$ method at defined positions on the surface of the top layer of the reference geometries [15,16]. Table 2 shows the parameters used for the residual stress analysis.

Table 2. Parameters for residual stress analysis using XRD ($\sin^2\psi$ method).

Radiation: CrKα	**Tube Power: 30 kV/6.7 mA**	**Collimator: 2 mm**	**Detector: Linear Solid State**
Diffraction Line: {211}α	ψ-Tilting: 0° to ±45°	ψ-Steps: ±10	Measuring Time: 5 s

3. Results and Discussion

3.1. Thermophysical Welding and Forming Simulation with Dilatometer

Figure 4 shows the ultimate tensile strength as a function of the cooling time $\Delta t_{8/5}$ for the test materials S690QL, S960QL, and WAAM wire.

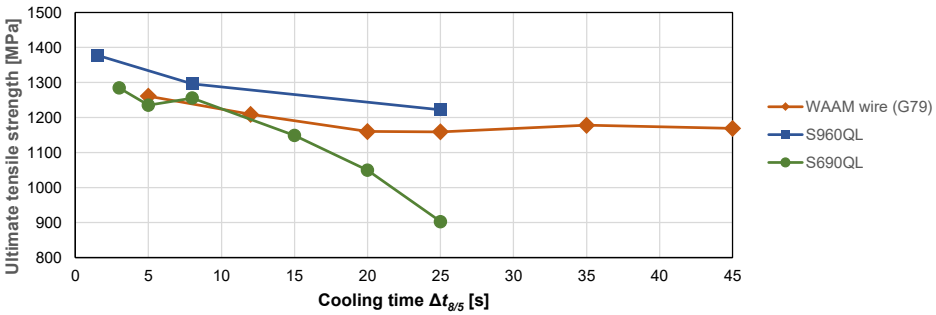

Figure 4. Influence of $\Delta t_{8/5}$ cooling time on ultimate tensile strength of the investigated test materials S690QL, S960OL, and high-strength WAAM wire (G79) with 3 experiments per data point and a maximum standard deviation $S = \pm 10$ MPa.

Between 5 s and 25 s, the tensile strength of all test materials decreased with increasing cooling time $\Delta t_{8/5}$. Due to the higher grade and the different alloying concept, the level of the strength determined for S960QL was comparatively higher than that of the other test materials. From approx. 10 s, the strength reduction increased significantly for S690QL compared to S960QL and the WAAM wire. The absolute difference between the maximum and minimum tensile strength for the S690QL over the entire $\Delta t_{8/5}$ time range was significantly higher (with 350 MPa) than for S960QL or G79, with a difference of approx. 150–200 MPa. This could be traced back primarily to the increased proportions of strength-increasing alloying elements compared to the S690QL steel, such as Ni, Mo, and Cr. From a cooling time of approx. 25 s, the ultimate tensile strength of the WAAM wire remained more or less constant up to 45 s. This was in accordance with studies of other authors, who focused on testing of mechanical properties in tensile specimens of an actual WAAM component/wall [14], in which, however, a relatively high effect of the cooling conditions on the yield strength was found. In future investigations, testing of the yield strength should therefore be mandatory.

Hence, the combination of S960QL as a substrate plate and such WAAM welding wire as a filler material would offer the potential of additive manufacturing in a wide $\Delta t_{8/5}$ time range without a significant loss in strength.

3.2. Cooling Time during Additive Manufacturing

As with multilayer welding, each WAAM layer is subject to a complex heat treatment consisting of multiple instances of heating and cooling (weld thermal cycle). The last effective cooling time $\Delta t_{8/5}$ with a peak temperature above 800 °C of the respective layer was relevant here. This last effective cooling rate significantly determined the microstructure and properties of the final component. Figure 5 shows the regression model of the determined $\Delta t_{8/5}$ times within the studied experimental design. The model quality was high, with $R^2 = 98.6\%$.

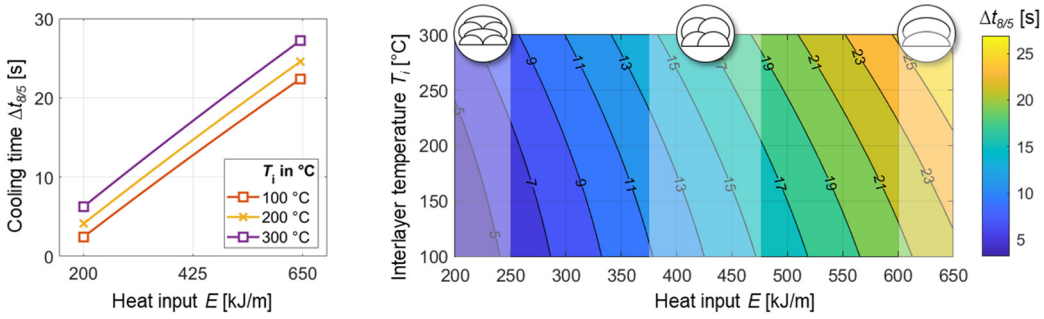

Figure 5. Cooling time $\Delta t_{8/5}$ as a function of heat input E and interlayer temperature T_i: effect diagram (**left**) and contour plot (**right**) of the quadratic regression model; model quality $R^2 = 98.6\%$.

The statistical evaluation showed (within a quadratic regression model) that the effects of the interlayer temperature and heat input were both significant. The cooling time increased approx. linearly with increasing heat input. Due to a slight interaction between the heat input and interlayer temperature, this linear increase could be observed at all interlayer temperatures. The heat input had a much stronger effect on the cooling time than the interlayer temperature, since there was a correlation with the amount of heat introduced, and thus had a major influence on the cooling characteristics of the component. Due to the rather low heat dissipation into the component, especially at higher layer numbers, the cooling time could only be adjusted to a small extent by varying the interlayer temperature at a constant heat input. It should be mentioned that this was in strong contrast to the effect of the interpass temperature on joint welding, which had a significantly higher influence on the cooling rates depending on the plate thickness and applied heat input, with which it also had a considerable interaction [7].

3.3. Residual Stress Analysis

Figure 6 shows the distribution of residual stresses on the top layer surface of the specimen, which was manufactured with central test parameters (E = 425 kJ/m, T_i = 200 °C).

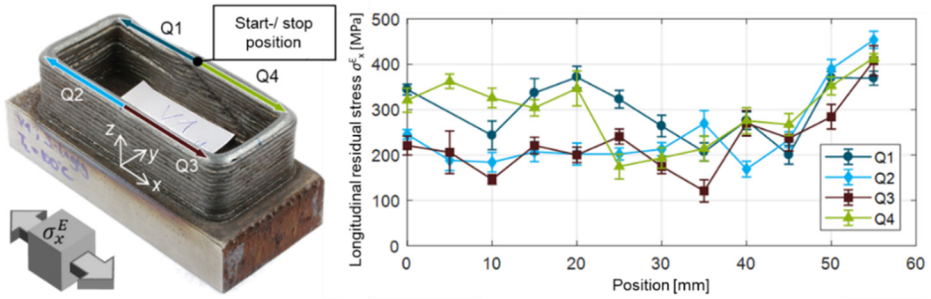

Figure 6. Residual stress distribution in welding direction $\sigma^E{}_x(x)$ on the top layer of the specimen welded with central test parameters (E = 425 kJ/m, T_i = 200 °C).

For this purpose, the specimens were divided into four quadrants (Q1 to Q4). The analysis proceeded from the centerline of the specimen (x = 0 mm) to the corners. A constant residual stress level in the middle area of the walls and an increase to approx. 400 MPa of the tensile residual stresses in the corner areas was exhibited that could be traced back to a higher design-related shrinkage restraint corresponding to commonly known models. These results were qualitatively comparable with other studies; e.g., on WAAM of IN718 [8,20]. However, the ratio of yield strength to residual stress was lower here. It was assumed that this was due to compensating transformation residual stresses (formation of compressive loads during cooling process) due to the solid-phase transformation of the high-strength steel weld metal according to generally accepted concepts [16,21]. Another influence on the residual stresses occurred due to the weld start and end points. An increased heat input in quadrants Q1 and Q4 at the weld start and end, respectively, caused elevated residual stresses compared to Q2 and Q3, where constant process conditions prevailed. The mean scatter of the analyzed stress values was ±22 MPa. To determine the influence of the heat input and interlayer temperature on the residual stresses of the surface layers, all nine WAAM-welded hollow cuboids were analyzed in the range of x = 0 mm to x = 35 mm. The mean residual stress level was determined in each case, cf. Figure 6. Figure 7 shows the statistical evaluation of the averaged stress levels from Q3 using regression analysis.

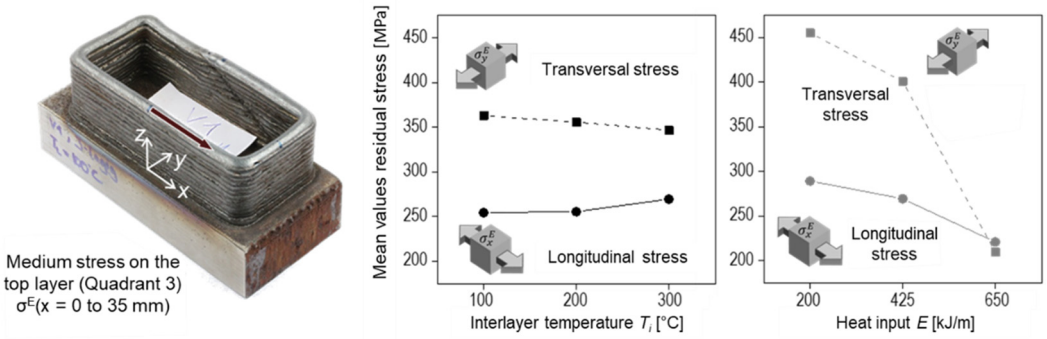

Figure 7. XRD analysis track on Q3 (**left**), influence of interlayer temperature (**center**), and heat input (**right**) on residual stresses σ^E longitudinally and transversely to the welding direction; averaged stresses on top layer within Q3. Model qualities: for σ^E_x: R^2 = 69.5%; for σ^E_y: R^2 = 88.7%.

The interlayer temperature (Figure 7, center) showed no significant influence on either the longitudinal or transversal local residual stresses of the top layer, as the effect on the cooling time also was rather small. The heat input (Figure 7, right) had a significant effect on the longitudinal residual stresses σ^E_x (p = 0.011). The model quality was R^2 = 69.5%. The increase in heat input caused a lower residual stress level on the top layer. This was due to the smaller cross-section of the top layer at a lower fusion rate, with a comparable shrinkage restraint due to the dimensions of the wall. Although this resulted in similar high shrinkage forces, they acted over a smaller cross-section compared to the higher deposition rate. The transversal residual stresses σ^E_y were also influenced by the heat input. The effect was significant (p = 0.005), with a model quality of R^2 = 88.7%. A comparable influence similar to the longitudinal residual stresses could be assumed, with the difference that the shrinkage restraint in the transverse direction (wall thickness direction) was much less pronounced than in the longitudinal direction.

It should be emphasized that the resulting residual stress level on the surface of the top layer was the result of a complex superposition of shrinkage, quenching, and transformation residual stresses according to general concepts, as mentioned above [21]. Other authors investigated these local effects due to high temperature gradients, and found significant influences on the local stress distributions and magnitudes [21], as well as complex interactions with superimposing global welding stresses due to high shrinkage restraints [7]. In comparison to other studies with materials that did not undergo a solid-phase transformation during cooling, which influenced the residual stresses; e.g., [8,20], there was an overall change in the stress equilibrium up to an overall reduction in the residual stresses, which can be specifically utilized, or is already systematically exploited by special material developments [22]. It is therefore important to clarify which of these effects dominates and contributes significantly to the local residual stress formation. This is ultimately reserved for further investigations. For this purpose, areal residual stress analyses on the side walls of the hollow cuboids, as well as exemplary stress analyses in the bulk, are planned.

4. Conclusions

This paper presented an influence analysis of the interlayer temperature and heat input on cooling time and residual stresses of high-strength steel components manufactured using WAAM. The results allowed the following conclusions:

1. New high-strength, special WAAM wires can be processed over a wide $\Delta t_{8/5}$ cooling time range (5–45 s) without a pronounced decrease in strength.
2. By adapting the layer build-up strategy, constant component geometries with a different heat input could be realized.
3. The heat input had a significant influence on the cooling behavior during layer-by-layer production of the component. High heat input values led to lower cooling rates.

The interlayer temperature had a comparatively small effect on the cooling time, and should thus be suitable for adjusting or optimizing in terms of the process time or stress engineering.

4. The residual stresses on the top layers along the welding direction showed an increase of over 50% (from approx. 200 MPa to up to 300–450 MPa) on average toward the corners of the part due to design-related restraints.
5. The interlayer temperature did not show any significant influence on the local residual stresses of the top layer surface within the experimental design.
6. The effect of heat input on the local longitudinal and transversal residual stress level on the top layer surfaces was significant. A higher heat input or fusion rate caused considerably lower residual stresses (e.g., $\Delta\sigma^{E}_{max} \geq 200$ MPa between E = 200 kJ/m and 650 kJ/m). A final clarification of these influences will require the investigation of local effects due to shrinkage and transformation caused by high local temperature gradients during cooling, as well as systematic investigations of other specimen surfaces, such as the specimen side walls; residual stresses analyses in the bulk are required for this purpose.

These results are the basis for ongoing investigations of the residual stress levels and distributions (e.g., side wall surface and bulk). Furthermore, the effect of component design and WAAM strategy and the resulting weld thermal cycle on the welding stresses, microstructure, and properties will be examined. These will help to derive recommendations regarding stress-optimized WAAM processing with high-strength steel filler metals and the development of an easy-to-apply cold-cracking test for WAAM.

Author Contributions: R.S.-W., A.H., K.W. and D.S. designed the experiment; R.S.-W. and A.H. carried out the welding tests, the thermophysical forming simulation with the dilatometer, and the evaluation of the data generated in the process; K.W. and D.S. were responsible for the planning, execution, and evaluation of all residual stress measurements; R.S.-W. wrote this article. J.H., A.K. and T.K. contributed to data evaluation, interpretation and discussion. All authors have read and agreed to the published version of the manuscript.

Funding: The IGF project No. 21162 BG (P 1380) of the Research Association for Steel Applications (Forschungsvereinigung Stahlanwendung e. V.) was funded by the German Federal Ministry for Economic Affairs and Climate Action via the German Federation of Industrial Research Associations (AiF) within the framework of the program for the promotion of joint industrial research (IGF) on the basis of a resolution of the German Bundestag. We would like to express gratitude for this funding, as well as for the cooperation and support of the companies and persons actively involved in the project advisory committee. The publication of this article was funded by Chemnitz University of Technology and by the Deutsche Forschungsgemeinschaft (DFG, German Research Foundation)—491193532.

Institutional Review Board Statement: Not applicable.

Informed Consent Statement: Not applicable.

Data Availability Statement: Not applicable.

Conflicts of Interest: The authors declare no conflict of interest.

References

1. Raoul, J. *Use and Application of High-Performance Steels for Steel Structures*; Guenther, H.-P., Ed.; IABSE: Zürich, Switzerland, 2005.
2. Hulka, K.; Kern, A.; Schriever, U. Application of Niobium in Quenched and Tempered High-Strength Steels. *Mater. Sci. Forum* **2005**, *500–501*, 519–526. [CrossRef]
3. European Commission. European Green Deal. 2021. Available online: https://ec.europa.eu/clima/eu-action/european-green-deal_en (accessed on 20 December 2021).

4. Plangger, J.; Schabhüttl, P.; Vuherer, T.; Enzinger, N. CMT Additive Manufacturing of a High Strength Steel Alloy for Application in Crane Construction. *Metals* **2019**, *9*, 650. [CrossRef]
5. Frazier, W.E. Metal additive manufacturing: A review. *J. Mater. Eng. Perform.* **2014**, *23*, 1917–1928. [CrossRef]
6. Ding, D.; Pan, Z.; Cuiuri, D.; Li, H. Wire-feed additive manufacturing of metal components: Technologies, developments and future interests. *Int. J. Adv. Manuf. Technol.* **2015**, *81*, 465–481. [CrossRef]
7. Schroepfer, D.; Kromm, A.; Schaupp, T.; Kannengiesser, T. Welding stress control in high-strength steel components using adapted heat control concepts. *Weld. World* **2018**, *63*, 647–661. [CrossRef]
8. Hoennige, J.; Seow, C.E.; Ganguly, S.; Xu, X.; Cabeza, S.; Coules, H.; Williams, S. Study of residual stress and microstructural evolution in as-deposited and inter-pass rolled wire plus arc additively manufactured Inconel 718 alloy after ageing treatment. *Mater. Sci. Eng. A* **2021**, *801*, 140368. [CrossRef]
9. Denkena, B.; Grove, T.; Stamm, S.; Vogel, N.; Nordmeyer, H. Verzug additiver Bauteile. Einfluss der Nachbearbeitung auf den Eigenspannungszustand. *Konstruktion* **2019**, *3*, 203–222.
10. Rodrigues, T.A.; Duarte, V.; Miranda, R.M.; Santos, T.G.; Oliveira, J.P. Current Status and Perspectives on Wire and Arc Additive Manufacturing (WAAM). *Materials* **2019**, *12*, 1121. [CrossRef] [PubMed]
11. Chen, X.; Chuanchu, S.; Yangfan, W.; Noor, S.A.; Konovalov, S.; Jayalakshmi, S.; Singh, R.A. Cold Metal Transfer (CMT) Based Wire and Arc Additive Manufacture (WAAM) System. *J. Surf. Investig. X-Ray Synchrotron Neutron Tech.* **2019**, *12*, 1278–1284. [CrossRef]
12. Graf, M.; Hälsig, A.; Höfer, K.; Awiszus, B.; Mayr, P. Thermo-Mechanical Modelling of Wire-Arc Additive Manufacturing (WAAM) of Semi-Finished Products. *Metals* **2018**, *8*, 1009. [CrossRef]
13. Ogino, Y.; Asai, S.; Hirata, Y. Numerical simulation of WAAM process by a GMAW weld pool model. *Weld. World* **2018**, *62*, 393–401. [CrossRef]
14. Mueller, J.; Hensel, J.; Dilger, K. Mechanical properties of wire and arc additively manufactured high-strength steel structures. *Weld. World* **2022**, *66*, 395–407. [CrossRef]
15. Withers, P.J.; Bhadeshia, H.K.D.H. Overview—Residual stress part 1—Measurement techniques. *Mater. Sci. Tech. Ser.* **2001**, *17*, 355–365. [CrossRef]
16. Withers, P.J.; Bhadeshia, H.K.D.H. Overview—Residual stress part 2—Nature and origins. *Mater. Sci. Tech. Ser.* **2001**, *17*, 366–375. [CrossRef]
17. Taraphdar, P.K.; Kumar, R.; Pandey, C.; Mahapatra, M.M. Significance of Finite Element Models and Solid-State Phase Transformation on the Evaluation of Weld Induced Residual Stresses. *Met. Mater. Int.* **2021**, *27*, 3478–3492. [CrossRef]
18. Sprengel, M.; Mohr, G.; Altenburg, S.J.; Evans, A.; Serrano-Munoz, I.; Kromm, A.; Pirling, T.; Bruno, G.; Kannengiesser, T. Triaxial Residual Stress in Laser Powder Bed Fused 316L: Effects of Interlayer Time and Scanning Velocity. *Adv. Eng. Mater.* **2022**. [CrossRef]
19. Kromm, A.; Cabeza, S.; Mishurova, T.; Nadammal, N. Residual Stresses in Selective Laser Melted Samples of a Nickel Based Superalloy. *Mater. Res. Proc.* **2018**, *6*, 259–264. [CrossRef]
20. Kumar, M.D.B.; Manikandan, M. Evaluation of Microstructure, Residual Stress, and Mechanical Properties in Different Planes of Wire + Arc Additive Manufactured Nickel-Based Superalloy. *Met. Mater. Int.* **2022**, 1–24. [CrossRef]
21. Nitschke-Pagel, T.; Wohlfahrt, H. Residual Stresses in Welded Joints—Sources and Consequences. *Mater. Sci. Forum* **2002**, *404–407*, 215–226. [CrossRef]
22. Dixneit, J.; Kromm, A.; Boin, M.; Wimpory, R.C.; Kannengiesser, T.; Gibmeier, J.; Schroepfer, D. Residual stresses of LTT welds in large-scale components. *Weld. World* **2017**, *61*, 1089–1097. [CrossRef]